Scripta Materialia 169 (2019) 9–13

Contents lists available at ScienceDirect

Scripta Materialia

journal homepage: www.elsevier.com/locate/scriptamat

Virtual bound states elements and their effects on magnetic and electrical properties of Fe-Ni based metal amorphous nanocomposites

N. Aronhime [a,*], P. Ohodnicki [b], M.E. McHenry [a]

[a] Carnegie Mellon University, Pittsburgh, PA 15213, United States of America
[b] National Energy Technology Laboratory, Pittsburgh, PA 15236, United States of America

ARTICLE INFO

Article history:
Received 18 March 2019
Received in revised form 1 May 2019
Accepted 2 May 2019
Available online 9 May 2019

Keywords:
Soft magnetic materials
Electrical properties

ABSTRACT

Metal amorphous nanocomposite alloys, with compositions $(Fe_{70}Ni_{30})_{80-x}Nb_4Si_2B_{14}TE_x$ ($0 \le x \le 5$), where TE is a transition element, and $(Fe_{70}Ni_{30})_{80-y}Nb_{4+y}Si_2B_{14}$ ($0.5 \le y \le 2$) were synthesized. Samples were annealed at 440 °C and strain-annealed at 440 °C and 300 MPa. Resistivity was found to increase with small substitutions of TE elements. Increasing V resulted in reduced B_s from 1.2 T to 0.5 T. Further Mo additions lowered B_s to 0.6 T, and consistently reduced the permeability. For Cr and Nb, resistivity increased, and strain-annealed permeability was lower than the annealed permeability. Lastly, toroidal core losses on $(Fe_{70}Ni_{30})_{79.5}Nb_4Si_2B_{14}V_1$ yielded W1.0/400 = 2.1 W/kg, and W1.0/1 k = 6.0 W/kg.

Metal amorphous nanocomposite (MANC) soft magnetic materials (SMM) promise increased efficiency and offer alternatives to reduce rare-earth (RE) metal use for electric motors. Recent hybrid motor designs, based on parallel path magnetics technology (PPMT) employ a RE permanent magnet as the rotor and cheaper high induction soft magnetic material as the stator [1,2]. A hybrid motor design based on RE-free permanent magnets and doubly salient stator and rotor as recently been reported with high power densities enabled by MANCs [3]. Laminated silicon steels have been traditionally used as a SMM in stators but newer materials can reduce motor size [1–3]. Recently developed advanced MANCs [4] can have usable peak inductions comparable to Si-steels with resistivities [5] that allow high switching frequencies required for high torques. High inductions and high frequency switching allows motor size reduction minimizing volume and weight, enabling new high efficiency motor topologies. This is leveraged on property improvements in MANCs targeting 1–10 kHz frequencies in geometries amenable to stators in high-speed motors [1,2]. While new MANC motors [1,2] consider Co-based MANCs due to the high temperature stability and attractive mechanical properties, lower cost substituents [6] and replacement of Co by Fe-, Ni-, and/or FeNi-based materials may significantly impact the economics of such motors [3].

In electric motor applications, high saturation inductions are desired, and in AC applications, high permeability and low switching losses are critical. Low switching losses allows for high frequency switching, which in turn allows motor size reduction while maintaining power output. One of the main sources of loss is from classical eddy currents. This power loss can be expressed:

$$P_e = bf^2B^2 \tag{1}$$

where the b prefactor is:

$$b = \frac{(\pi \cdot t)^2}{\rho} \tag{2}$$

In Eq. (1), f is frequency and B is saturation induction. In Eq. (2), t is laminate thickness, and ρ is resistivity. It is clear that in order to minimize losses, small thickness and high resistivity are required. The other two sources of losses are hysteretic and anomalous eddy current losses. These three sources can be combined and mathematically represented by the well know Steinmetz [7] equation:

$$P = kf^{\alpha}B_m^{\beta} \tag{3}$$

where k, α, and β are fitting parameters, f is frequency, and B_m is the maximum induction.

The need to increase resistivity for use in AC currents is what originally prompted the development of Si-steels [8] which have typical resistivities around 50 μΩ-cm [9]. Si-steels are typically run at frequencies up to 400 Hz, above which different materials must be used. MANCs provide higher resistivities due to the residual amorphous phase, and this allows their use in the kHz frequency range. Beyond the resistivity gains from the amorphous phase, a further method of increasing the resistivity of an alloy is by adding virtual bound states (VBS).

* Corresponding author.
E-mail address: naronhim@andrew.cmu.edu (N. Aronhime).

https://doi.org/10.1016/j.scriptamat.2019.05.003
1359-6462/

VBS additions have shown resistivities of 180 μΩ-cm [10] in FeCo-based alloys, and have enhanced the resistivity and altered the magnetic properties of Co-based nanocomposites [11]. VBS theory describes a dilute transition element (TE) d-electron as it moves through the Fermi energy of a parent alloy comprised of late transition metals (TL), and is added to empty spin states [12,13]. Each TE atom will make contribution to the empty TL 3d states. This will have the side effect however of lowering the saturation induction of the alloy. The VBS TE atoms generate perturbing energy wells that scatter conduction electrons, thereby raising the resistivity. Impurity VBS have been described with a Lorenzian density of states (DOS) function:

$$g_i(\varepsilon) = \frac{5}{\pi}\frac{\Delta}{(\varepsilon-\varepsilon_d)^2+\Delta^2} \tag{4}$$

$$\Delta = \frac{2\pi}{\hbar|V_{sd}|^2} g_h(\varepsilon_d) \tag{5}$$

where Δ is the resonant state broadening, g_h is the host DOS, ε_d is the impurity d-state energy, and V_{sd} is the free electron scattering potential. In this work, we examine the effects of adding V, Cr, Mo and additional Nb to $(Fe_{70}Ni_{30})_{80}Nb_4Si_2B_{14}$ on resistivity, crystallization products, and magnetic properties.

Ingots with composition of $(Fe_{70}Ni_{30})_{80\text{-}x}Nb_4Si_2B_{14}TE_x$ ($0 \le x \le 5$), (TE = Cr, V, Mo), and $(Fe_{70}Ni_{30})_{80\text{-}y}Nb_{4+y}Si_2B_{14}$ ($0.5 \le y \le 2$) were produced by melting stoichiometric amounts of the constituent elements (purity of at least 99.8%) in a Miller arc-melter. The glass former composition was based on early transition metal [14] and metalloid [15] optimization. The ingots were cast into a ribbon using planar flow casting with an Edmund-Buhler Melt Spinner SC outfitted with a Cu-alloy wheel with an Ar atmosphere. The ribbons were determined to be amorphous by first employing a bend test of ductility [16] and then by XRD using a PANalytical X'Pert PRO. Strain annealing was accomplished by suspending the ribbon through a Thermolyne tube furnace with a set point of 440 °C and with a load hanging from one end. The load was such that the applied stress was 300 MPa. Magnetic hysteresis was measured with a Laboratorio Elettrofisico Single Strip Tester with a maximum field of 500 A/m for most samples. The B-H loops were measured at 50 Hz. Crystallization products were determined using the PANalytical X'Pert PRO XRD on the air side of the ribbon. A toroidal core was wound, and annealed at 440 °C. Losses were then measured on a Laboratorio Elettrofisico Hysteresisgraph with a variety of maximum inductions and frequencies. Transmission electron microscopy (TEM) experiments were performed using a High Angle Annular Dark Field Detector in a Tecnai F20 operating at 200 kV. Cross-sectional TEM samples spanning from the ribbon surface and into the bulk were prepared by standard Focused Ion Beam lift-out procedures from the wheel side of the ribbon.

Resistivity as a function of nominal % V, % Cr, % Nb, and % Mo is illustrated in Fig. 1. From the V series, it can be seen that resistivity initially increases with increasing V. From 1% V to 3.5% V, the resistivity remains constant within the error of the measurement. Above 3.5%, resistivity increases again, however, as discussed below, this increase is accompanied by a significant worsening of magnetic properties. Analyzing the V series using a three phase resistivity model [5], it is likely that the V is initially concentrated in the dispersed crystalline phase, which causes the initial resistivity rise. Once the crystal resistivity is comparable to or above the resistivity of the shell and amorphous phase, the resistivity

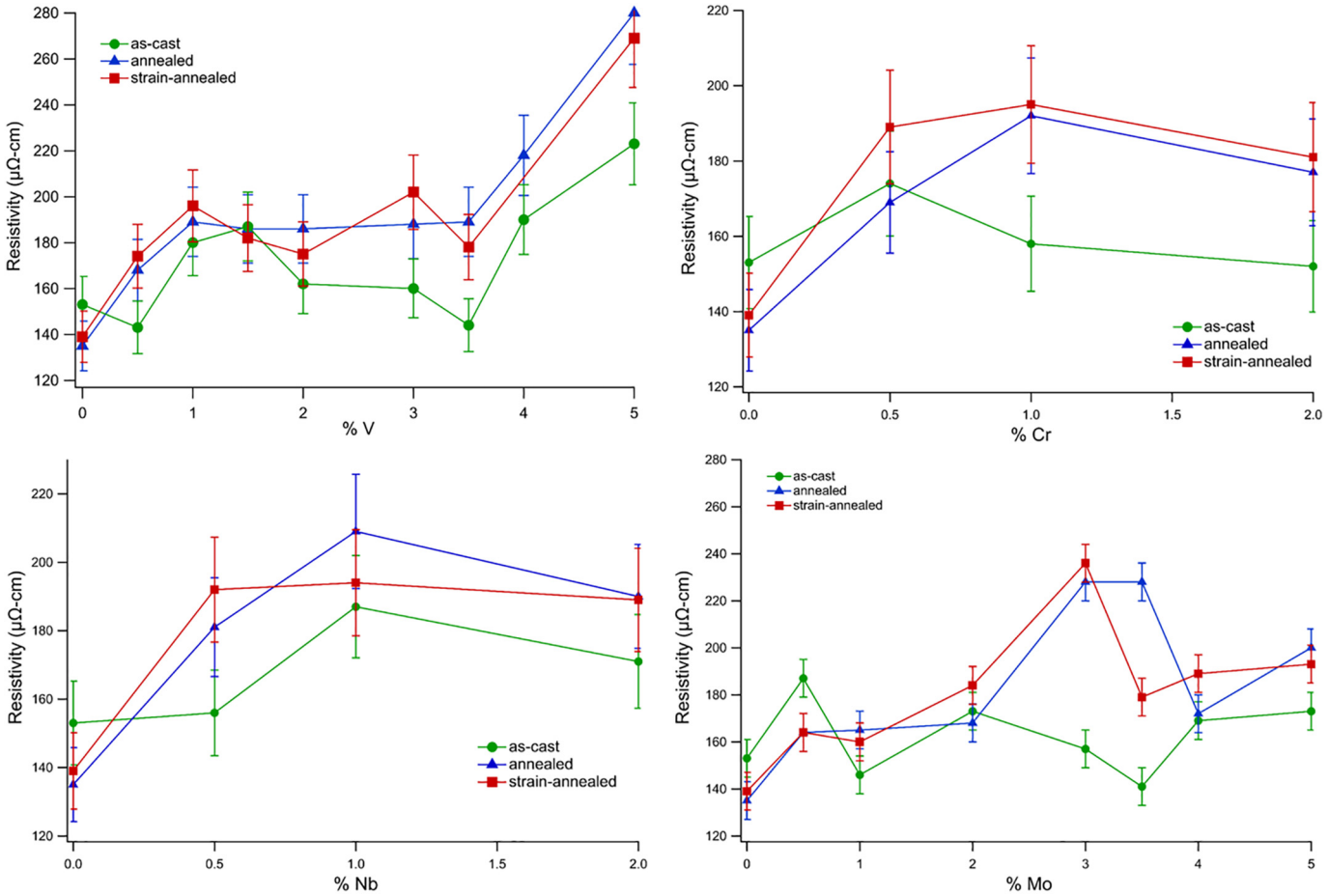

Fig. 1. Resistivity of V, Cr, Nb, and Mo series.

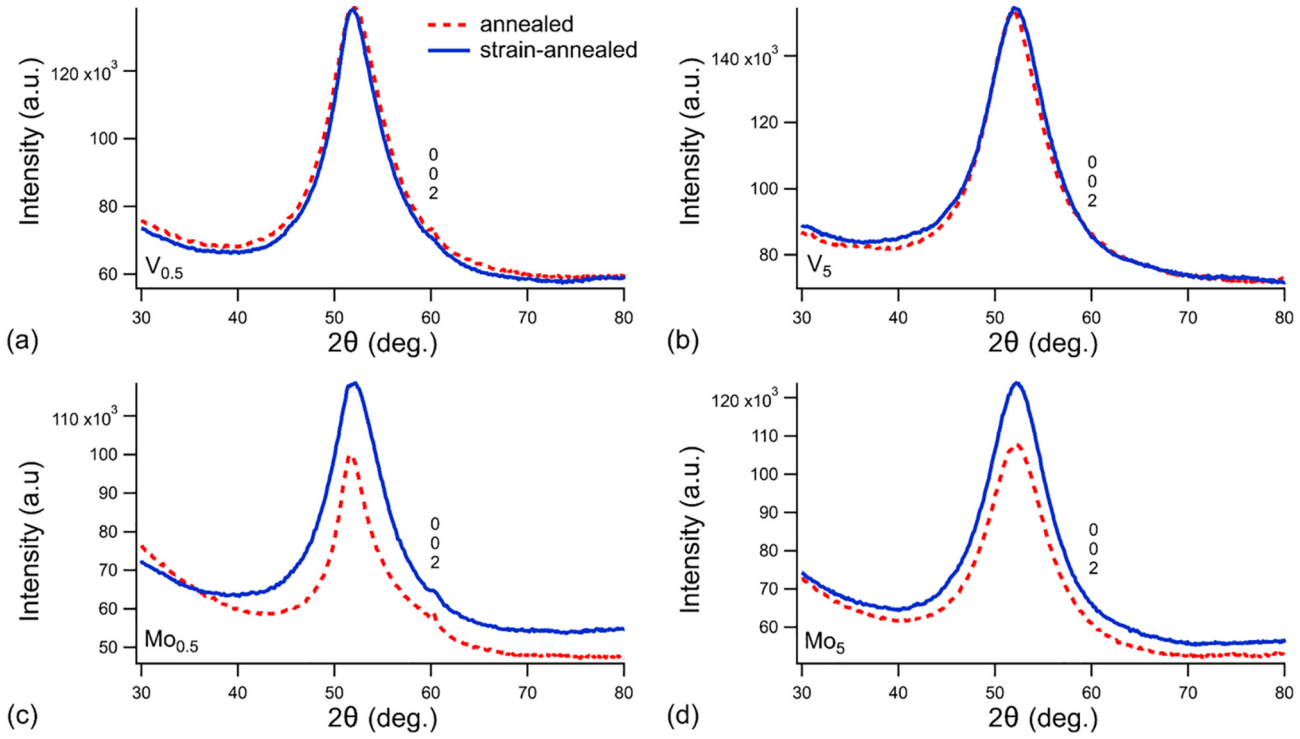

Fig. 2. XRD of $V_{0.5}$, V_5, $Mo_{0.5}$, and Mo_5.

remains constant as it is controlled by the amorphous phase and shell structure. The final rise in resistivity is postulated to be tied to the crystalline phase saturating with V, causing additional V to reside in the amorphous phase, further increasing the resistivity. The Cr and Nb series are both similar to the V series in that resistivity peaks at 1%, followed by a relative plateau beyond that. However, since the base alloy already has Nb in it, we expect any additional Nb to reside in the shell phase and/or the amorphous matrix.

In the Mo series, the resistivity increases with increasing Mo until 3% Mo, and then decreases. However, the as-cast Mo alloys have nearly constant resistivity. Since Mo is a large atom, it is expected to have low solubility in crystalline Fe-Ni, and will therefore accumulate in the shell structure around the crystals after annealing as is seen for other MANC growth inhibitors.

There has been significant work in other MANC systems tuning the growth inhibitor species and concentrations to optimize properties. For example, in FINEMET systems, Nb and several other early transition metal species have been attempted including Mo, Ta and W [17]. It was concluded that alloys with Nb exhibited the best soft magnetic properties, in alloys with crystal size <40 nm, thereby minimizing the coercivity. Partial replacement of Nb with Mo in FINEMET type compositions was found to increase H_C [18,19]. Similarly, with HITPERM alloys and with Co-based alloys, H_C was lower with Nb rather than Zr or Hf used as the glass former [20–24].

It is also worth considering how these atoms effect the Fe phase diagram at elevated temperatures. Ni, Co, V, Cr, Mo and Nb are all alloying elements known to expand the γ-loop in iron and steels. The binary Fe-Co system exhibits a continuous γ-phase field for temperatures in excess of ~950 °C [25,26]. The binary Fe-Ni system exhibits a continuous γ-phase field for temperatures in excess of ~912 °C. For Ni concentrations in excess of ~20 at.% the γ-phase is stable to temperatures below 600 °C [27]. However, the γ➔α phase transformation is sluggish and a metastable γ-phase can be retained for much lower Ni concentrations even in nanostructures [28]. Typically solubilities of 2–3 at.% for V, Nb, Mo and 10–11 at.% for Cr, are possible in equilibrium as maximum solubilities (at temperature in excess of 1000 °C) in the γ-loop.

In the ternary Fe-Co-V system exhibits a continuous disordered α-phase field for temperatures in excess of 630 °C for 3 at.% V, giving evidence to the role of V as a stabilizing the disordered bcc phase in Fe-Co alloys and to the range of V solubility in the high temperature γ-phase [29,30]. A similar role in close-packed Fe-Ni phases would also retard ordering and provide VBS scattering both of which increase resistivity subject to solubility limits [12]. Mo is well known trace alloying addition to permalloys and Fe-rich, γ-FeNi nanoparticles [31].

X-ray diffraction scans of $(Fe_{70}Ni_{30})_{79.5}Nb_4Si_2B_{14}V_{.5}$, $(Fe_{70}Ni_{30})_{75}Nb_4Si_2B_{14}V_5$, $(Fe_{70}Ni_{30})_{79.5}Nb_4Si_2B_{14}Mo_{.5}$, and $(Fe_{70}Ni_{30})_{75}Nb_4Si_2B_{14}Mo_5$ can be seen in Fig. 2. In general, there is no appreciable difference between annealed and strain-annealed scans. The main peak at 52° is an overlap of the residual amorphous phase, and fcc [111]. However, a small fcc [002] peak is also observed. The XRD scans for the Cr and Nb series are nearly identical, with a broad mixed amorphous and [111] peak, and a small fcc [002] peak observed.

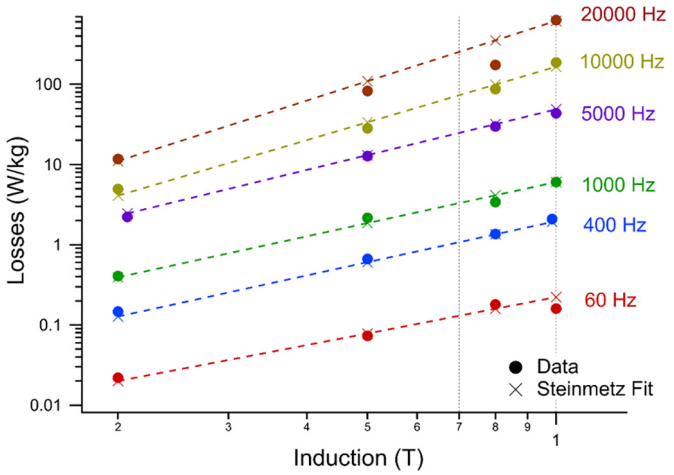

Fig. 3. Toroidal core losses in $(Fe_{70}Ni_{30})_{79}Nb_4Si_2B_{14}V_1$.

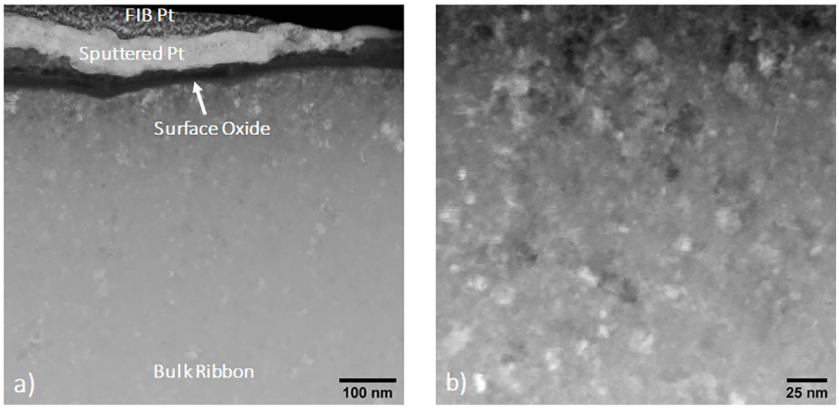

Fig. 4. Cross-sectional STEM images prepared for an $(Fe_{70}Ni_{30})_{80}Nb_4Si_2B_{14}$ MANC alloy after a 440 °C annealing treatment on the wheel side of the ribbon. a) Wheel side surface illustrating surface oxide layers of ~15–100 nm in thickness depending on the location.

Permeability was measured for all annealed and strain annealed samples. It should be noted that previous permeability measurements of the base alloy yielded μ_r of 4000 and 16,000 for annealed and strain-annealed treatments respectively [32]. The addition of VBS elements quickly changes this trend of increasing μ_r with strain-annealing. In fact, in almost all the samples tested, permeability is lower for the strain-annealed sample than for the annealed sample. This is likely due to changing the magnetostriction coefficient, λ, which is often a metric for the sign and magnitude of the strain-induced anisotropy associated with residual stresses present after primary crystallization in BCC-based MANCs [33]. In previously studied FCC Co-based MANCs[11] large decreases in permeability to as low as ~5 are observed and associated with sizeable anisotropy induced by growth faults and attributed to the role of VBS elements in reducing the stacking fault energies in Co. Such a phenomenon is not observed in FeNi-based MANCs and while strain annealing reduces permeabilities, they remain above 2000. It is anticipated that at higher frequencies the benefits of reduced eddy current losses may outweigh loss in permeability in motor applications. It is worth noting that the mechanism of permeability tuning in these Fe-Ni alloys is unknown and is under investigation.

Increasing permeability would be indicative of parallel (along the ribbon direction) induced anisotropy, while decreasing permeability is indicative of transverse induced anisotropy. In the V series, once V exceeds 3%, the saturation induction, B_S, is reduced to 0.5 T, from an induction >1 T in the base alloy. In addition, there is a significant increase in the coercivity at 5% V. In the Mo series, B_S decreases from 3% Mo to 5% Mo to a minimum value of 0.6 T. However, there is no appreciable change in the coercivity. Likewise in the Cr and Nb series, there was no change in coercivity.

Toroidal losses were measured on $(Fe_{70}Ni_{30})_{79}Nb_4Si_2B_{14}V_1$ due to its high resistivity and high induction. Losses at six frequencies as a function of induction can be seen in Fig. 3. The k, α, and β values range from 2 to 2.6, 1.15–1.25, and 1.5–2.5 respectively. The losses at 1 T, 400 Hz and 1 kHz are comparable to recently published Fe-based MANC losses [34], and are significantly lower than 3% Si-steel [35,36] and 6.5% Si-steel [36]. However, these losses are somewhat higher than Metglas 2605SA1 [34], $(Fe_{70}Ni_{30})_{80}Nb_4Si_2B_{14}$ [32], and another Fe-based MANC, $Fe_{89}Hf_7B_4$ [35].

In addition to the electrical conductivity within the ribbon plane, another source of eddy current losses is observed in tape wound cores when significant electrical conductivity exists between adjacent laminations. Additional insulation layers are not typically introduced on the surface of commercially available MANC alloys. However, electrical insulation results from the presence of a native oxide layer which forms during the rapid solidification and subsequent annealing stages. An example of the native oxide which forms on the wheel side of an $(Fe_{70}Ni_{30})_{80}Nb_4Si_2B_{14}$ alloy is presented in Fig. 4a showing an ~15–100 nm surface oxide which varies in thickness across the ribbon surface. In the bulk of the ribbon, the expected nanocrystalline microstructure is clearly observed as shown in Fig. 4b.

Metal amorphous nanocomposite alloys were made of composition $(Fe_{70}Ni_{30})_{80-x}Nb_4Si_2B_{14}TE_x$ $(0 \le x \le 5)$ and $(Fe_{70}Ni_{30})_{80-y}Nb_{4+y}Si_2B_{14}$ $(0.5 \le y \le 2)$. Samples were annealed at 440 °C and strain-annealed at 440 °C and 300 MPa. Resistivity was found to increase with small amounts of TE elements. For V, further increases resulted in reduced B_S from 1.2 T to 0.5 T, lower permeability, and higher H_C. For Mo, further additions lowered B_S to 0.6 T, and consistently reduced the permeability of strain-annealed ribbon, but had a smaller effect on the permeability of annealed ribbon. For Cr and Nb series, resistivity increased, and strain-annealed permeability was lower than the annealed permeability. There was no systematic worsening of B_S or H_C. XRD scans revealed residual amorphous phase, and fcc Fe-Ni peaks. Lastly, toroidal core losses on $(Fe_{70}Ni_{30})_{79.5}Nb_4Si_2B_{14}V_1$ yielded $W_{1.0/400} = 2.1$ W/kg, and $W_{1.0/1k} = 6.0$ W/kg, slightly larger than alloys without V.

Acknowledgements

The authors acknowledge support from the DOE Solar Energy Technology Office and the Grid Modernization Laboratory Consortium through the SuNLaMP initiative under Agreement #DE-EE-00031004. MEM acknowledges support from the DOE AMO program through DOE/EERE Office of Advanced Manufacturing Program Award Number: DE-EE0007867.

References

[1] J.M. Silveyra, A.M. Leary, V. DeGeorge, S. Simizu, M.E. McHenry, J. Appl. Phys. 115 (2014) 17A319.
[2] J.M. Silveyra, P. Xu, V. Keylin, V. DeGeorge, A. Leary, M.E. McHenry, J. Electron. Mater. 45 (2016) 219–225.
[3] S. Simizu, P.R. Ohodnicki, M.E. McHenry, IEEE Trans. Magn. PP (2018) 1–5.
[4] M.E. McHenry, M.A. Willard, D.E. Laughlin, Prog. Mater. Sci. 44 (1999) 291–433.
[5] V. Degeorge, S. Shen, P. Ohodnicki, M. Andio, M.E. McHenry, J. Electron. Mater. 43 (2014) 96–108.
[6] M. Kurniawan, V. Keylin, M.E. McHenry, J. Mater. Res. 30 (2015).
[7] C.P. Steinmetz, Am. Inst. Electr. Eng. Trans. 3 (1892) 3.
[8] J. Hopkinson, Philos. Trans. R. Soc. Lond. 176 (1885) 455–469.
[9] https://Cogent-Power, Com (2004).
[10] M.S. Lucas, W.C. Bourne, A.O. Sheets, L. Brunke, M.D. Alexander, J.M. Shank, E. Michel, S.L. Semiatin, J. Horwath, Z. Turgut, Mater. Sci. Eng. B 176 (2011) 1079–1084.
[11] A. Leary, V. Keylin, A. Devaraj, V. DeGeorge, P. Ohodnicki, M.E. McHenry, J. Mater. Res. 23 (2016) 1–19.
[12] M.E. McHenry, D.E. Laughlin, 19 - Magnetic Properties of Metals and Alloys, Fifth Edit, Elsevier B.V, 2015.
[13] J. Friedel, Nuovo Cim. 7 (1958).
[14] K.J. Miller, A. Leary, S.J. Kernion, A. Wise, D.E. Laughlin, M.E. McHenry, V. Keylin, J. Huth, J. Appl. Phys. 107 (2010) 09A316.
[15] S.J. Kernion, K.J. Miller, S. Shen, V. Keylin, J. Huth, M.E. McHenry, IEEE Trans. Magn. 47 (2011) 3452–3455.

[16] M. Daniil, P.R. Ohodnicki, M.E. McHenry, M.A. Willard, Philos. Mag. 90 (2010) 1547–1565.
[17] Y. Yoshizawa, K. Yamauchi, Rapidly Quenched Mater. (1991) 176–179.
[18] D. Muraca, J. Silveyra, M. Pagnola, V. Cremaschi, J. Magn. Magn. Mater. 321 (2009) 3640–3645.
[19] J.A. Moya, V. Cremaschi, H. Sirkin, Phys. B Condens. Matter 389 (2007) 159–162.
[20] M.A. Willard, D.E. Laughlin, M.E. McHenry, D. Thoma, K. Sickafus, J.O. Cross, V.G. Harris, J. Appl. Phys. 84 (1998).
[21] J.. Blázquez, V. Franco, C.. Conde, A. Conde, J. Magn, Magn. Mater. 254–255 (2003) 460–462.
[22] P.R. Ohodnicki, J. Long, D.E. Laughlin, M.E. McHenry, V. Keylin, J. Huth, J. Appl. Phys. 104 (2008), 113909.
[23] A.M. Leary, V. Keylin, P.R. Ohodnicki, M.E. McHenry, J. Appl. Phys. 117 (2015) 17A338.
[24] H. Iwanabe, B. Lu, M.E. McHenry, D.E. Laughlin, J. Appl. Phys. 85 (1999).
[25] T. Nishizawa, K. Ishida, Bull. Alloy Phase Diagr. 5 (1984) 250–259.
[26] Z.A. Matysina, M.I. Milyan, Diagr. Sostoyan v Mater. Khim. Termodinum I Term. Anal (1991) 100–107.
[27] L.J. Swartzendruber, V.P. Itkin, C.B. Alcock, J. Phase Equilib. 12 (1991) 288–312.
[28] J.J. Ipus, P. Herre, P. Ohodnicki, M.E. McHenry, J. Appl. Phys. 111 (2012).
[29] V. Raghavan, J. Phase Equilib. 23 (2002) 442.
[30] Z. Turgut, R.T. Fingers, H.R. Piehler, M.E. McHenry, IEEE Trans. Magn. 36 (2000) 3024–3025.
[31] H. Ucar, M. Craven, D.E. Laughlin, M.E. McHenry, J. Electron. Mater. 43 (2014) 137–141.
[32] N. Aronhime, V. DeGeorge, V. Keylin, P. Ohodnicki, M.E. McHenry, JOM 69 (2017) 2164–2170.
[33] G. Herzer, V. Budinsky, C. Polak, J. Phys. Conf. Ser. 266 (2011).
[34] K. Suzuki, R. Parsons, B. Zang, K. Onodera, H. Kishimoto, A. Kato, Appl. Phys. Lett. 110 (2017), 012407.
[35] K. Suzuki, A. Makino, A. Inoue, T. Masumoto, J. Appl. Phys. 74 (1993) 3316–3322.
[36] C.-W. Chen, Magnetism and Metallurgy of Soft Magnetic Materials, Dover Publications, Amsterdam, 1986.